# Effect of potential shape and excitation spectrum on power harvested from ambient vibration



by
Jasmine H. Chan

SUBMITTED TO THE DEPARTMENT OF MECHANICAL ENGINEERING IN PARTIAL
FULFILLMENT OF THE REQUIREMENTS FOR THE DEGREE OF

BACHELOR OF SCIENCE IN MECHANICAL ENGINEERING
AT THE
MASSACHUSETTS INSTITUTE OF TECHNOLOGY

FEBRUARY 16, 2015 [June 2015]



Signature of Author: Signature redacted
Department of Mechanical Engineering
February 16, 2015

Certified by: Signature redacted
Konstantin Turitsyn
Professor of Mechanical Engineering
Thesis Supervisor

Accepted by: Signature redacted
Anette Hosoi
Professor of Mechanical Engineering
Undergraduate Officer

# Effect of potential shape and excitation spectrum on power harvested from ambient vibration

by
Jasmine H. Chan

Submitted to the Department of Mechanical Engineering
on February 16, 2015 in Partial Fulfillment of the
Requirements for the Degree of Bachelor of Science in
Mechanical Engineering

ABSTRACT

In recent years, there have been experimental developments in energy harvesting from ambient vibrations in small-scale sensing. The ultimate goal is to replace batteries in these sensors. Linear systems have a narrow bandwidth, but ambient vibrations occur over a potentially broad range of frequencies. Nonlinear systems—in particular, bistable systems—have a wide bandwidth. The objective of this thesis is to understand the dependence of power harvested on the shape of the potential–in the transition from linear to bistable. A single degree-of-freedom mathematical model was developed and simulated in MATLAB over varying operating conditions and potential function parameters. The findings from this thesis support experimental results that nonlinearity improves the amount of power that is harvested.

Thesis Supervisor: Konstantin Turitsyn
Title: Professor of Mechanical Engineering

**Acknowledgements**

I would like to thank my Thesis Supervisor, Professor Konstantin Turitsyn from the Department of Mechanical Engineering at the Massachusetts Institute of Technology. His guidance over the past one and a half years, and in particular the last six months, has been among the most influential experiences I have had during my undergraduate years. I would also like to thank Ashkan Haji Hosseinloo, one of Professor Turitsyn's graduate students, for his assistance, guidance, and availability during the last couple weeks.

## Contents

## List of Figures

## 1 Introduction

The desire to efficiently harvest energy from ambient vibrations is increasing with the prevalence of small electronics. Eventually, sufficiently efficient and small energy harvesters will be able to replace the batteries in small electronics. Initial research into vibrational energy harvesting began with linear systems, but research has moved to the nonlinear system [3].

Linear energy harvesters are tuned to have resonant frequency at the dominant ambient frequency. At this frequency, the linear energy harvester is most efficient [4–6]. However, an excitation frequency that deviates from the resonant frequency of the system results in a drastic decrease in harvesting efficiency [6–8]. This narrow bandwidth that is characteristic of a linear harvester can not recover the energy that can be harvested from frequencies that are present but are out of range. Several solutions have been presented to solve the problem of the narrow frequency bandwidth: active tuning, arrays of cantilevers, and frequency up-conversion [4, 6, 9].

Active tuning involves a constant adjustment of the resonant frequency of the mechanical system to match the excitation frequency [10–12]. A cantilever array is comprised of a series of cantilevers, each with a different natural frequency [13]. This increases the frequency bandwidth of the harvester. Frequency up-conversion is based on the premise that because the excitation and resonant frequencies are different, the mechanical system developed uses some mechanism to up-convert the excitation frequency [14]. For example, Külah and Najafi have achieved frequency up-conversion through the use of magnets and a cantilever beam [14].

While operating a linear harvester at resonance is most efficient, there are several drawbacks. For example, for linear systems with low damping, the resonant frequency peak is very sharp and further exacerbates the issue of the narrow frequency bandwidth of high efficiency harvesting [15]. Another problem that arises in vibrational energy harvesting is the small scale of the systems. As the size of the linear harvester decreases, the higher the natural frequency. However, ambient frequencies are in the range of 1 to 100 Hz [14, 16], much too low for the physical constraints of the system.

In order to widen the bandwidth of the energy harvester, it has been proposed that a nonlinear energy harvester is more practical and more efficient for a broad range of frequencies [5–7, 17, 18]. Many experimental and mathematical models that bistable nonlinear oscillators are effective over a wider frequency range significantly below the structure's resonant frequency than linear oscillators [1, 3, 4, 6, 19, 20]. Methods used to examine the effect of nonlinearity on harvesting capability include both experimental and theoretical analysis [3]. An example technique commonly implemented is the use of magnets: by placing a magnet at the tip of the cantilever beam and a magnet in the cantilever housing, it is possible to alter the motion of the cantilever beam to be nonlinear [2].

A common form of a nonlinear energy harvester that broadens the bandwidth of the generator is the bistable structure [1, 4]. Three of the most common configurations for achieving bistable dynamics can be seen in Figure 1: a repulsive magnet, a pair of attractive magnets, and a buckled beam [1]. A bistable system allows for three modes of oscillation: small limit cycle oscillations (intrawell), chaotic motion with potential barrier crossing between intrawell oscillations, and large limit cycle oscillations (interwell) (see Figure 2) [1, 16]. From experimentation, a bistable harvester exhibiting interwell oscillations will yield grater levels of output power but chaotic oscillations did not yield a substantial increase in voltage

output [1, 8].

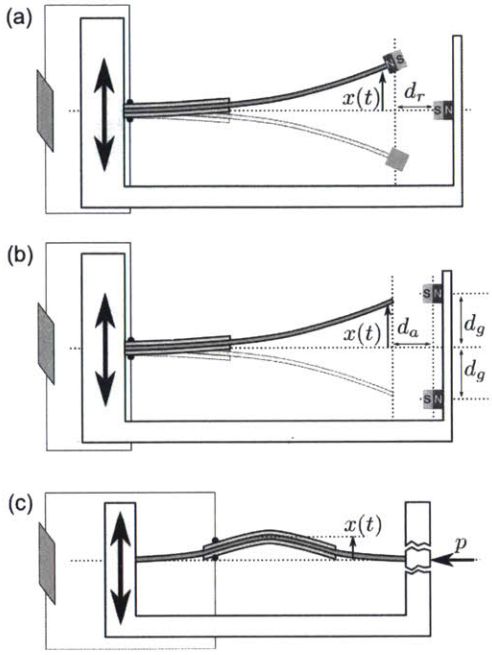


**Figure 1:** Three common designs for creating a bistable system: a) repulsive magnets at the tip of the cantilever and fixed to the housing; b) attractive magnets at the tip of the cantilever and fixed to the housing; and c) a buckled beam [1].

This thesis investigates the effect of bistable dynamics on the average power that can be harvested. The force potential of the oscillator used was a fourth degree polynomial described in the Harne and Wang review [1]. By using MATLAB to simulate the dynamics of the system and to calculate the average power, it was shown that the most power can be harvested during the transition between monostable and bistable systems. This result confirms the experimental findings by Tang, Yang, and Soh [16], that the most power can be harvested during the transition between linear monostable and bistable systems.

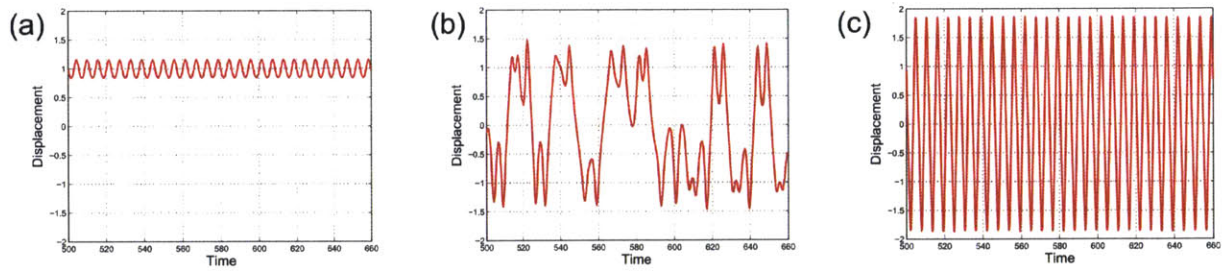


**Figure 2:** Depicted are the three modes of oscillation: a) intrawell oscillations; b) chaotic oscillations, and; c) interwell oscillations [1].

## 2 Mathematical model

A second order differential equation with a nonzero external force was used to model the harvester. The governing equation is given below

$$\ddot{x} + 2\zeta\dot{x} + \frac{dU(x)}{dx} = F(t) \tag{1}$$

where $x$ is the relative displacement of an inertial mass, $\zeta$ is the damping ratio, $U(x)$ is the potential function of the mechanical system, $F(t)$ is the external force (Eq. 2), and the overdot represents differentiation with respect to time. In this thesis, there are three cases of excitation force. Case 1 where $n = 1$; Case 2 where $n = 2$; and Case 3 where $n = 10$. The forcing function was calculated by

$$F(t) = \sum_{i=1}^{n} \sin(\omega_i t) \tag{2}$$

Two types of potential functions were used in this simulation: a linear monostable potential function and a bistable potential function. The monostable potential function is a linear dynamical system, described in Section 2.1; the bistable potential function is a nonlinear dynamical system, described in Section 2.2.

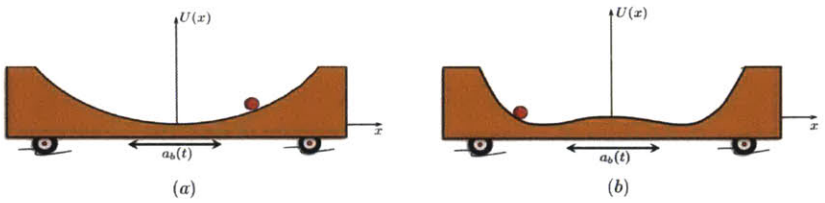


**Figure 3:** A linear and bistable system modeled as a particle on a moving cart: a) monostable potential; and, b) bistable potential [2].

The motion of a linear potential versus the motion of a bistable potential can be visualized using a cart model (see Figure 3). The surface of the cart is the same as the graph of the potential function. The cart moves laterally at an acceleration analogous to the external force in Eq. 2. The response of the spherical particle on the cart is the relative displacement between the sphere and the line of symmetry.

Average power ($\overline{P}$) is calculated using the mean energy dissipated by the system at steady state. The average energy dissipated, $E = \zeta \int \dot{x}^2 dt$, at steady state is the average power multiplied by the change in time:

$$\overline{P} = \frac{E}{t} = \frac{\zeta \int \dot{x}^2 dt}{t} \tag{3}$$

### 2.1 *Linear harvester*

The linear energy harvester has a potential function that is a second order polynomial. In this case, the linear potential function is:

$$U_{lin}(x) = \frac{N_1}{2}(1-r)x^2 \tag{4}$$

where $N_1$ is the linear stiffness and $r$ is a tuning parameter. Substituted into Eq. 1, the governing differential equation for the system becomes:

$$\ddot{x} + 2\zeta\dot{x} + N_1(1-r)x = F(t) \tag{5}$$

$N_1$ is related to the natural frequency, $\omega_n$, by $N_1 = \omega_n^2$, and represents the linear stiffness of the material used for harvesting. Linear energy harvesters are typically tuned to the strongest ambient frequency in order to maximize the harvested power, as linear harvesters are most efficient when the excitation frequency is very close to the natural frequency [6–8].

### 2.2 *Linear-bistable transition and bistable harvester*

A single degree-of-freedom bistable oscillator has a restoring force potential

$$U_{bistable}(x) = \frac{N_1}{2}(1-r)x^2 + \frac{N_3}{4}x^4, \tag{6}$$

where $N_1$ and $N_3$ represent linear and nonlinear stiffness, respectively, and r is a tuning parameter. As $N_1$ and $N_3$ increase, the potential wells deepen as shown in Figure 4. Substituting Eq. 6 into Eq. 1, the differential equation governing the dynamics of a bistable energy harvester is

$$\ddot{x} + 2\zeta\dot{x} + N_1(1-r)x + N_3x^3 = F(t) \tag{7}$$

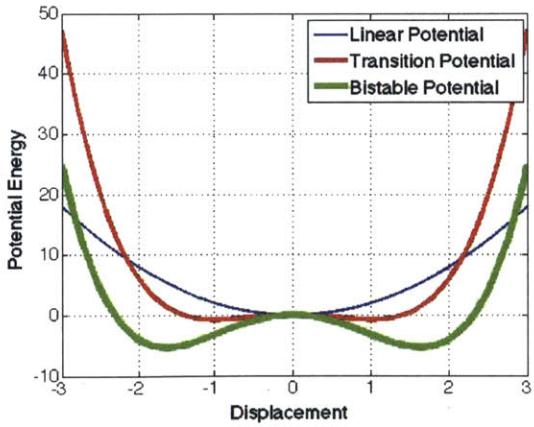


**Figure 4:** Sample potential functions as $N_1$, $N_3$, and $r$ vary. For the monostable potential, $r = 0$ and $N_3 = 0$. For both the transition and the bistable potentials, $r = 1$ and $N_1, N_3 > 0$. $N_1$ and $N_3$ in the bistable case are greater than in the transition case.

## 3 Simulation and analysis

Three cases of excitation force were simulated in MATLAB in order to understand the effect of bistability on the harvested power. The first case was harmonic forcing at one frequency (Section 3.2). The second case was harmonic forcing at two frequencies (Section 3.3). The third case was random forcing over the frequency range of 1 to 100 Hz (Section 3.4). The linear response was also simulated for $N_1 = 4$, $N_3 = 0$, and $r = 0$ in each case. In each case, the linear and nonlinear stiffnesses were varied over a range of values that yielded stable potentials. $N_1$ was varied between values of 2 and 8; and $N_3$ was varied between values of 2 and 4, for $r = 2$. Figure 5 shows the four extrema of the $N_1$ and $N_3$ variations and the linear potential function.

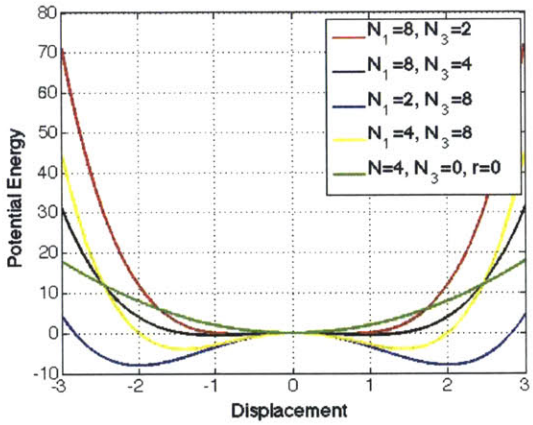


**Figure 5:** The five graphs above show the potential function of the extrema of the range of $N_1$ and $N_3$, and the linear potential function simulated in this thesis. $r = 2$ unless specified otherwise in the legend.

ode45() was the ordinary differential equation solver provided by MATLAB that was used to solve the dynamical system. ode45() uses a Runge-Kutta-based numerical integration technique. The initial conditions were set to start at one unit left of the left-most stable point of the potential. The solution was calculated for time values between 0 and 150. The forcing amplitude was 8. The damping ration was $\zeta = 0.1$. The energy of the system was calculated by extending the solver function. The MATLAB code is printed in Appendix A.

### *3.1 Linear responses*

This section includes the time-history of the linear solutions in each case and brief discussion on the responses. The potential function parameters for each simulation were $N_1 = 4$, $N_3 = 0$, and $r = 0$. Case 1 was simulated at a frequency of 20 Hz,. Case 2 was simulated at excitation frequencies of 25 and 45 Hz. Case 3 was simulated using ten randomly selected (by the randi() function in MATLAB) frequencies between 1 and 100 Hz.

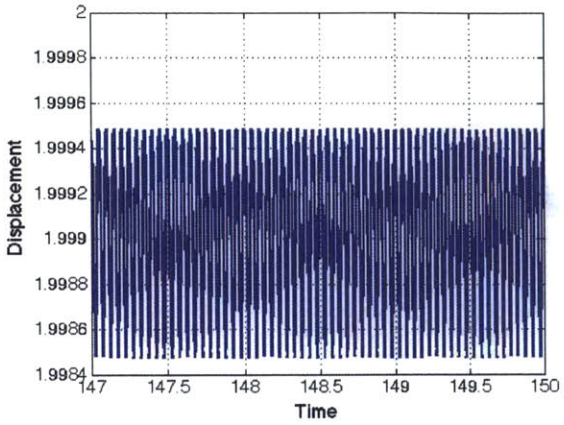


**(a)** Case 1: Linear response with $\omega =$ 20Hz. The linear response oscillates at the forcing frequency at steady state.

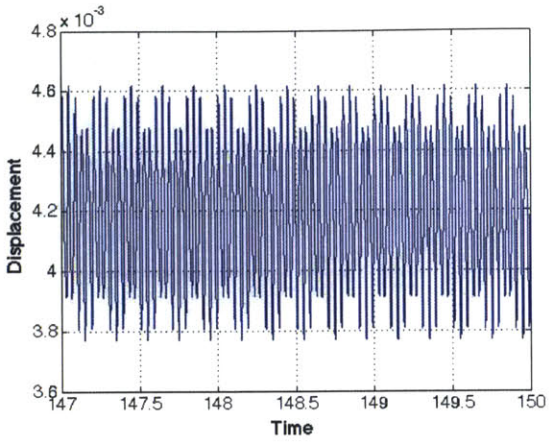


**(b)** Case 2: Linear response with $\omega_1 =$ 25Hz and $\omega_2 =$ 45Hz. The response consists of a slow and a fast oscillation.

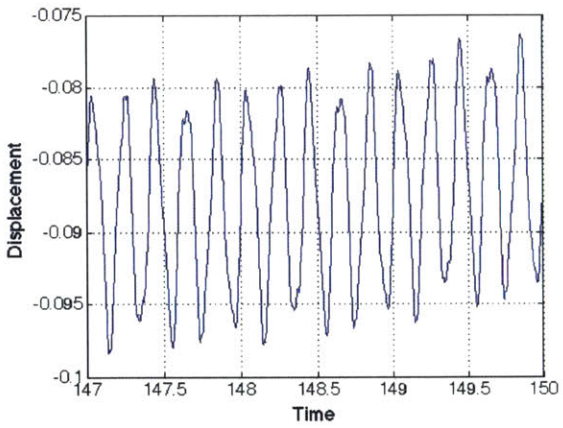


**(c)** Case 3: Linear response with $n =$ 10 values of $\omega$ between 1 and 100 Hz. Many oscillation frequencies can be seen adding together in this solution.

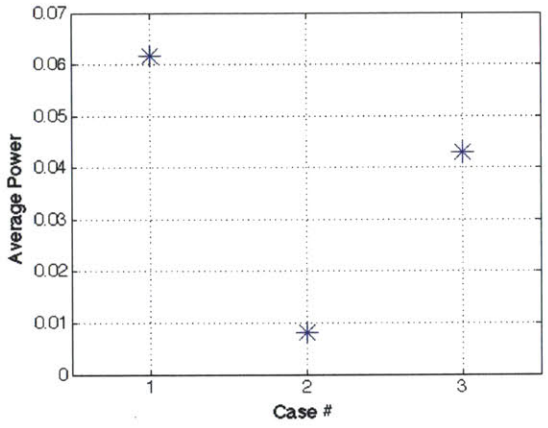


**(d)** Power harvested in each of the former three cases described. Case 1: 0.0617, Case 2: 0.0081, Case 3: 0.0428.

**Figure 6:** Time histories of the linear system and the power harvested during each case.

Figures 6a to 6c are the time histories of the linear responses at steady state. The response depicted in Figure 6a is oscillating at 20 Hz, which is expected of a linear system. There are two frequencies present in Figure 6b with fast oscillations contained within slow oscillations. The oscillations present in Figure 6c is wider and appears to have an underlying slow oscillation as well. For each case, the power harvested was also calculated. These values can be seen in Figure 6d.

### 3.2 *Case 1: Harmonic forcing*

The first case was simulated using a single excitation frequency at 20 Hz. This frequency was chosen arbitrarily from the range of frequencies typical for ambient vibrations, 1 to 100 Hz. In this case, $r = 1$. Selected results from the simulation of the single frequency harmonic forcing are presented and discussed below.

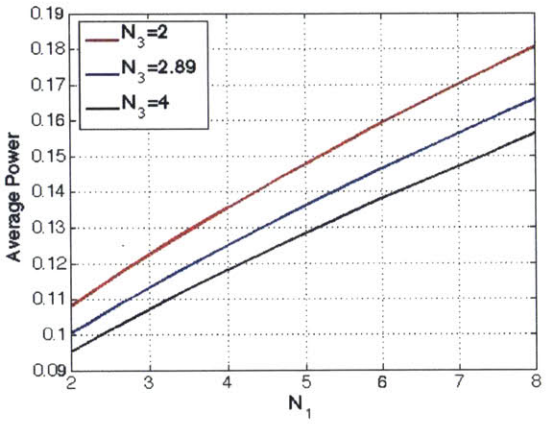


**(a)** Power dependence on linear stiffness for several values of nonlinear stiffness. Power and linear stiffness are directly proportional.

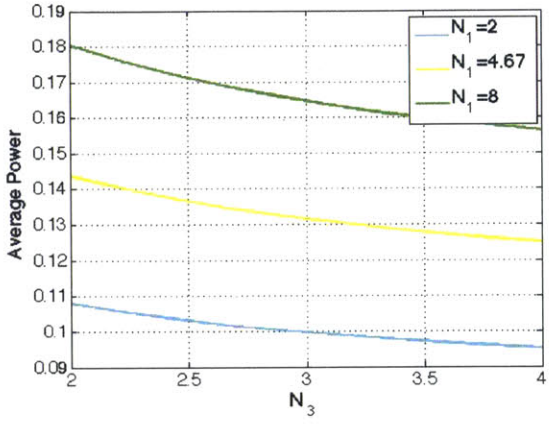


**(b)** Power dependence on nonlinear stiffness for several values of linear stiffness. Power and nonlinear stiffness are inversely proportional.

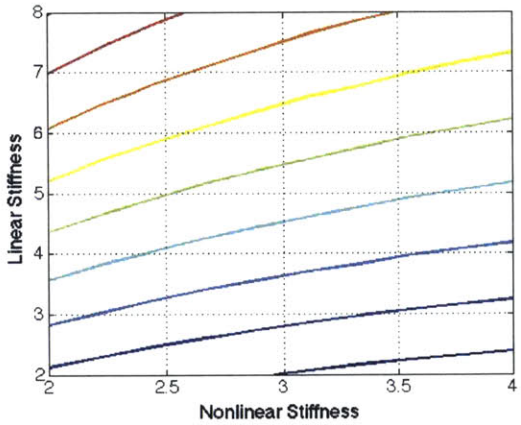


**(c)** Contour plot of power harvested on both linear and nonlinear stiffness.

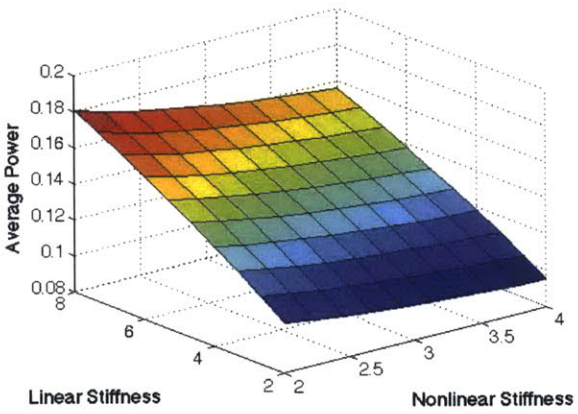


**(d)** Surface plot of power harvested versus linear and nonlinear stiffness.

**Figure 7:** Case 1 Results: the most power is harvested for high linear stiffness and low nonlinear stiffness.

Figure 7 depicts the dependence of harvested power on $N_1$ and $N_3$. From Figure 7a, as $N_1$ increases the average power also increases. $N_1$ is related to the linear stiffness and physically

represents the clamping or stiffening of the mechanical structure that is dissipating the energy. This result suggests that the natural frequency is approaching the excitation frequency. For values of $N_1$ that cause the natural frequency to exceed the excitation frequency, the linear spring has been overstiffened and does not oscillate much under the excitation force.

Figure 7b suggests that as the nonlinear stiffness of the potential increases, the less power is harvested. This result is consistent with experimental results found by Tang, Yang and Soh: the transitional period between a linear monostable system and a nonlinear bistable system dissipates the most energy [16].

Figure 8 was plotted using the $N_1$ and $N_3$ values that were the extrema of the harvested power in Figure 7d. The red potential function corresponds with the system with the greatest harvested average power. This result also agrees with the experimental results.

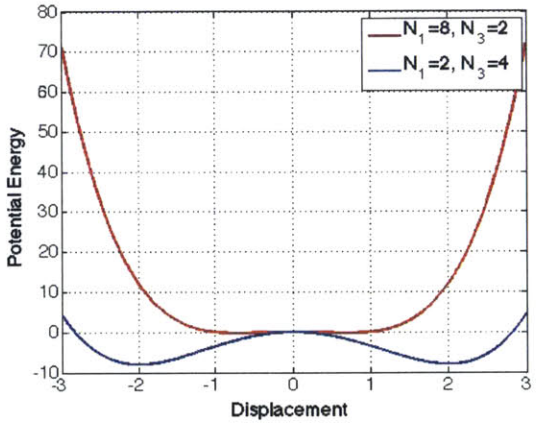


**Figure 8:** Case 1: potential functions from the extrema of power harvested (see Figure 7d). Note that the monostable potential harvested more energy than the bistable potential harvested.

While this simulation confirms the findings of Tang, Yang, and Soh, it is still unclear, theoretically, why this is the case. Conceptually, however, it is almost an intuitive result. As the potential function changes from linear to bistable, the basin of attraction widens before the two wells begin to form. This wide basin appears to eliminate the first and second modes of oscillations (intrawell and chaotic oscillations, see Figure 2).

The power harvested by a linear system under the same excitation force was 0.0617. From Figure 7b, the power harvested is at least between 0.1 and 0.14 as $N_3$ approaches zero for $N_1 = 4$. The power harvested using a nonlinear system is far greater. In the case of single frequency harmonic forcing, the simulation suggests that a wide potential function with a linear stiffness that is close to the excitation frequency is most effective.

### *3.3 Case 2: Harmonic forcing with two frequencies*

This section covers analysis of the simulation of harmonic forcing at two frequencies. The two frequencies were 25 and 45 Hz. As in Case 1, the two frequencies were chosen arbitrarily from between 1 and 100 Hz. The results of the simulation are presented below in Figure 9.

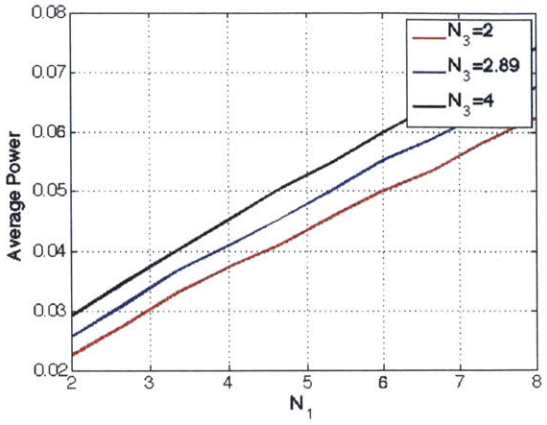


**(a)** Power dependence on linear stiffness for several values of nonlinear stiffness. Power and linear stiffness are directly proportional.

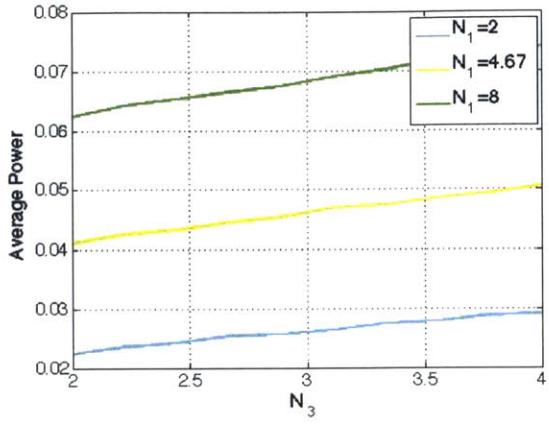


**(b)** Power dependence on nonlinear stiffness for several values of linear stiffness. Power and nonlinear stiffness are directly proportional.

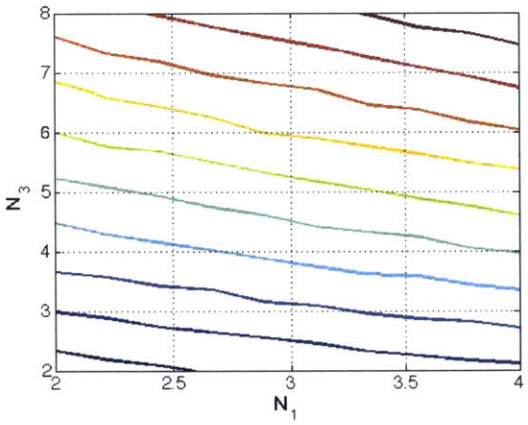


**(c)** Contour plot of power harvested on both linear and nonlinear stiffness.

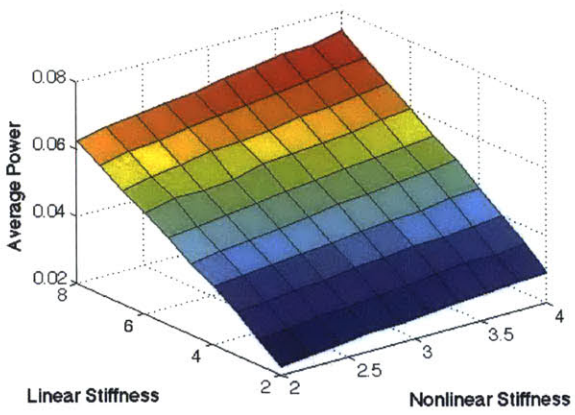


**(d)** Surface plot of power harvested on both linear and nonlinear stiffness.

**Figure 9:** Case 2 Results: the most power is harvested for low linear stiffness and high nonlinear stiffness.

Figure 9 depicts the dependence of harvested power on $N_1$ and $N_3$. Both Figures 9a and 9b show a positive correlation between linear stiffness, nonlinear stiffness, and average power. The trend for the average power versus linear stiffness remained the same between Case 1 and Case 2. This consistence suggests that the assumption made about the cause of the increasing power for increasing $N_1$ may be an accurate conclusion.

However, the trend for the average power versus nonlinear stiffness flips for Case 2. For two excitation frequencies, increasing nonlinearity benefits the power that can be harvested from the system. Figure 10 shows the two potential functions that correspond with the extrema on the graph in Figure 9d. This result is in opposition with the results that Tang, Yang, and

Soh present. In their paper, Tang, Yang, and Soh only present results for harvested power from one excitation frequency [16].

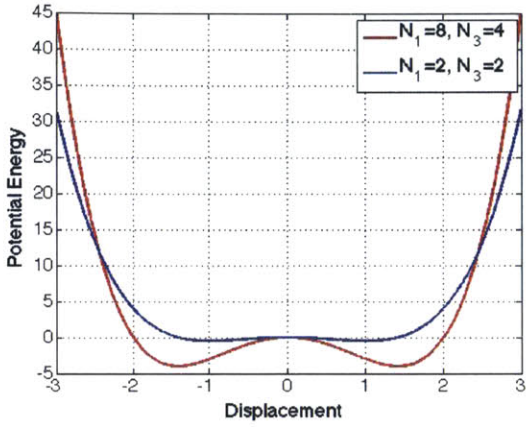


**Figure 10:** Two potential functions that correspond with the power extrema. The red graph corresponds with the $N_1$ and $N_3$ combination that harvested the most power. The blue graph corresponds with the least power harvested.

The power harvested by a nonlinear system is greater than the power harvested by a linear system. For the linear case solved in Section 3.1, the power harvested was 0.0081, whereas Figure 9b suggests that as $N_3$ approaches 0 for $N_1 = 4$, the average power is between 0.03 and 0.04, significantly greater than the power harvested by the linear system. The optimal configuration for two excitation frequencies is to have relatively high linear and nonlinear stiffnesses.

### *3.4 Case 3: White noise*

This section will cover analysis of simulation for forcing the system at multiple randomly selected frequencies using the randi function in MATLAB. There were 10 frequencies randomly selected by randi() in MATLAB between 1 and 100 Hz. The results of the simulation are presented below in Figure 11.

Figure 11 shows the dependence of harvested power on $N_1$ and $N_3$. The power harvested by changing $N_3$ converges (see Figure 11a) and increasing $N_3$ has no effect on the power harvested (Figure 11b). This result does not mirror the experimental results.

Figure 12 depicts the potential functions that are at the extremal contour lines of Figures 11c and 11d. Figure 12a corresponds with the maximum average power and Figure 12b corresponds with the minimum average power. These simulated results suggest that for a wide range of equally strong frequencies, nonlinear stiffness does not play a role in the power harvesting capability of the system and that the linear stiffness is the determining factor for this capability.

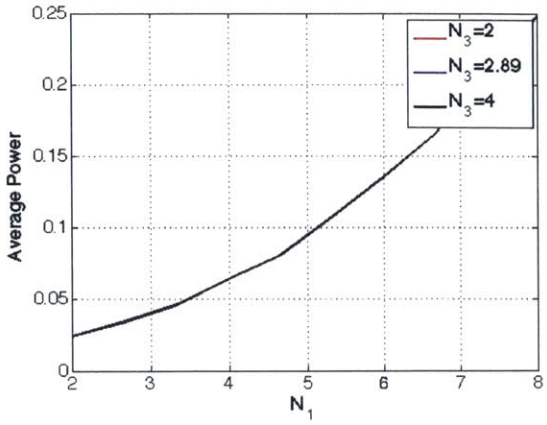


**(a)** Power dependence on linear stiffness for several values of nonlinear stiffness. Power and linear stiffness are directly proportional.

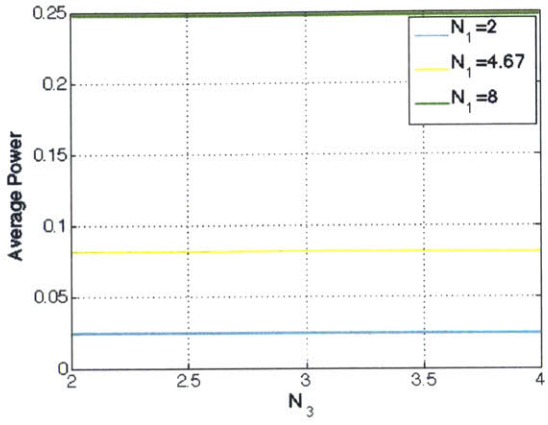


**(b)** Power dependence on nonlinear stiffness for several values of linear stiffness. Harvested power is independent of nonlinear stiffness.

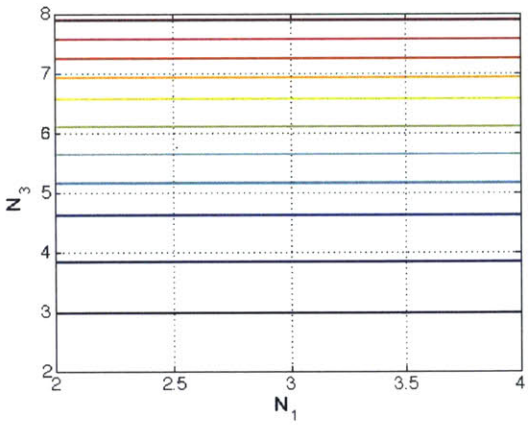


**(c)** Contour plot of power harvested on both linear and nonlinear stiffness.

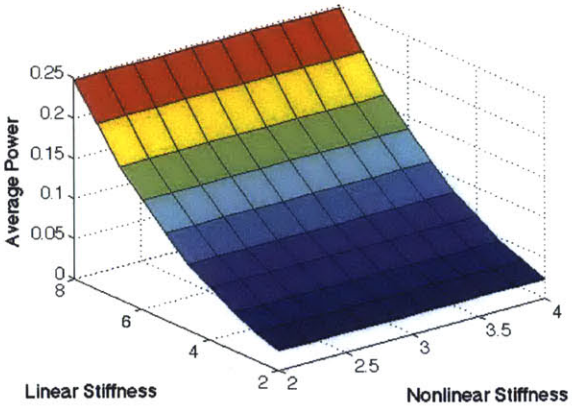


**(d)** Surface plot of power harvested on both linear and nonlinear stiffness.

**Figure 11:** Case 3 Results: the most power is harvested at high linear stiffness.

The linear response was calculated in Section 3.1 for $N_1 = 4$, $N_3 = 0$, and $r = 0$ and resulted in harvested power that is less than an extrapolated value from Figure 11a. The independence of the system on $N_3$ as $N_1$ varies shows that $P_{ave} \approx 0.06$ but the calculated value from the linear system is 0.0482. In this case, the optimal configuration is still to have some nonlinear component present in the system despite the calculated independence of the power on nonlinear stiffness.

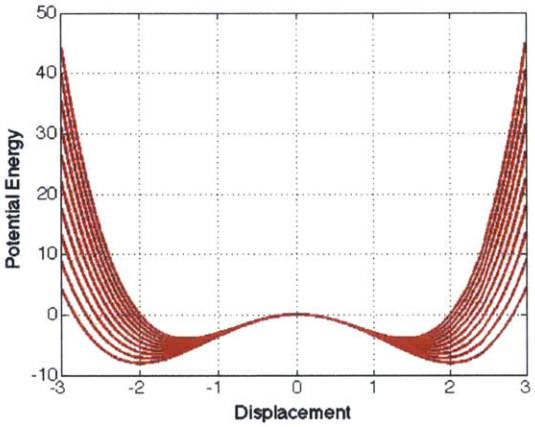


**(a)** Potential functions for the maximal power harvested.

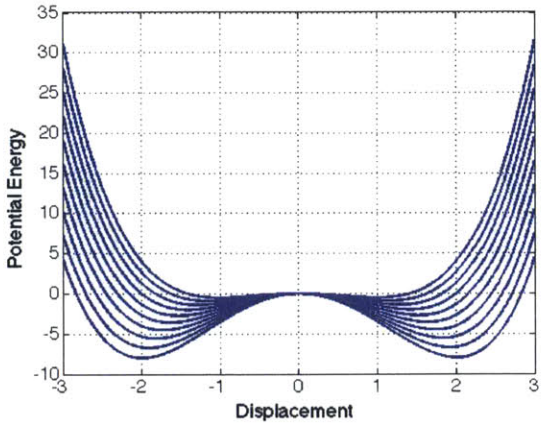


**(b)** Potential functions for the minimal power harvested.

**Figure 12:** Case 3: potential functions from the extrema of power harvested.

## 4 Conclusions

This thesis presents preliminary research into the effect of the potential shape on the energy harvested from ambient vibrations. In each case presented, the nonlinear system harvested more power than the linear system. However, in Cases 1 and 2, increasing linear stiffness also played a role in improving the amount of power harvested by the system. The effect of the linear stiffness over the range presented above suggests that the linear stiffness will constructively add to the harvested power.

Results from Case 1 supported the conclusions reached in Tang, Yang, and Soh, that the most power is harvested in the transition phase from a monostable to a bistable system. However, results from Cases 2 and 3 suggest that this conclusion is only valid when there is only one excitation frequency present. The results from Case 3 show that nonlinear stiffness may not be influential when the system is excited by multiple frequencies at the same amplitude over a large bandwidth.

Each case requires more extensive and detailed research. In particular, extending the range of both linear and nonlinear stiffnesses to test the hypothesis that above some critical linear stiffness, the power harvested will decrease due to overstiffening. This thesis covers information that is useful but not a full analytical explanation as to the nonlinear phenomena that occur in these transition and bistable systems. One method to understand and predict harvested power is perturbation analysis in order to characterize the effect of nonlinear stiffness and to provide qualitative reasoning for the results.

## 5 Appendix: MATLAB Code

MATLAB code for Cases 1-3, and the monostable case:
Case 1:

```
clc;
clear all;
global zeta;
global omega_forcing;
global N_1;
global N_3;
global r;
zeta = 0.1; %dimensionless damping constant
n=10;
N_1_1 = linspace(2,8,n);
N_3_1 = linspace(2,4,n);
r = 2;
omega_f_all_1 = 20*2*pi; %convert to rad/s forcing frequency; arbitrary
% potential function
x1 = (-3:0.0001:3);
Y_U1 = zeros(length(x1),n,n);
y_eq1 = zeros(n,n);
x_eq1 = zeros(n,n);
ind1 = zeros(n,n);
initial_conditions = zeros(n,4,n);
for j=1:n;
  for k = 1:n;
    Y_U1(:,j,k) = N_1_1(j)*(1-r)/2*x1.^2+N_3_1(k)/4*x1.^4;
    [y_eq1(j,k),ind1(j,k)] = min(Y_U1(:,j,k));
    x_eq1(j,k) = x1(ind1(j,k));
    initial_conditions(j,:,k) = [0,x_eq1(j,k)-1,0,0];
  end
end
% solving the differential equation
tau_values = [0 150];
total_E = zeros(n,n);
P_ave = zeros(n,n);
for i = 1:n;
  N_1 = N_1_1(i);
    for l = 1:n;
    N_3 = N_3_1(l);
    omega_forcing = omega_f_all_1;
    initial_condition = initial_conditions(i,:,l);
    [tv,yv] = ode45(@nonlin_corr_Case1,tau_values,initial_condition);
    yv_length = length(yv);
    total_E(i,l) = mean(yv(yv_length*0.75:yv_length,4));
```

```
        P_ave(i,l) = total_E(i,l)/tau_values(2);
      end
    end
```

Case 2:

```
    clear all;
    clc;
    %establish global variables and initialize
    global zeta;
    global omega_forcing1;
    global omega_forcing2;
    global N_1;
    global N_3;
    global r;
    zeta = 0.1; %dimensionless damping constant
    n=10;
    N_1_2 = linspace(2,8,n);
    N_3_2 = linspace(2,4,n);
    r = 2;
    omega_forcing1 = 25*2*pi; %convert to rad/s
    omega_forcing2 = 45*2*pi;
    % potential function
    x2 = (-3:0.0001:3);
    Y_U2 = zeros(length(x2),n,n);
    y_eq2 = zeros(n,n);
    x_eq2 = zeros(n,n);
    ind2 = zeros(n,n);
    initial_conditions = zeros(n,4,n);
    for j = 1:n;
      for k = 1:n;
        Y_U2(:,j,k) = N_1_2(j)*(1-r)/2*x2.^2+N_3_2(k)/4*x2.^4;
        [y_eq2(j,k),ind2(j,k)] = min(Y_U2(:,j,k));
        x_eq2(j,k) = x2(ind2(j,k));
        initial_conditions(j,:,k) = [0,x_eq2(j,k)-1,0,0];
      end
    end
    % solving the ODE
    tau_values = [0 100];
    total_E2 = zeros(n,n);
    P_ave2 = zeros(n,n);
    for i = 1:n;
      for l = 1:n;
        N_1 = N_1_2(i);
        N_3 = N_3_2(l);
        initial_condition = initial_conditions(i,:,l);
```

```
    [tv2,yv2] = ode45(@nonlin_corr_Case2,tau_values,initial_condition);
    yv_length2 = length(yv2);
    total_E2(i,l) = mean(yv2(yv_length2*.75:yv_length2,4));
    P_ave2(i,l) = total_E2(i,l)/tau_values(2);
  end
end
```

Case 3:

```
clear all;
clc;
%establish global variables and initialize
global zeta;
global N_1;
global N_3;
global omega_forcing;
global r;
global n_1;
zeta = 0.1; %dimensionless damping constant
n=10;
N_1_3 = linspace(2,8,n);
N_3_3 = linspace(2,4,n);
r = 2;
n_1 = 10;
omega_forcing = 2*pi*randi(100,n_1,1);
x3 = (-3:0.001:3);
Y_U3 = zeros(length(x3),n);
y_eq3 = zeros(n);
x_eq3 = zeros(n);
ind3 = zeros(n);
initial_conditions = zeros(n,4,n);
% potential function
for j = 1:n;
  for k = 1:n;
    Y_U3(:,j,k) = N_1_3(j)*(1-r)/2*x3.^2+N_3_3(k)/4*x3.^4;
    [y_eq3(j,k),ind3(j,k)] = min(Y_U3(:,j,k));
    x_eq3(j,k) = x3(ind3(j,k));
    initial_conditions(j,:,k) = [0,x_eq3(j)-1,0,0];
  end
end
tau_values = [0 100];
total_E3 = zeros(n,n);
P_ave3 = zeros(n,n);
for i = 1:n;
  for l = 1:n;
    initial_condition = initial_conditions(i,:,l);
```

```
        N_1 = N_1_3(i);
        N_3 = N_3_3(i);
        [tv3,yv3] = ode45(@nonlin_corr_Case3,tau_values,initial_condition);
        yv_length3 = length(yv3);
        total_E3(i,l) = mean(yv3(yv_length3*0.75:yv_length3,4));
        P_ave3(i,l) = total_E3(i,l)/tau_values(2);
      end

Linear Simulation:    clear all;
  clc;
  %set-up for all
  global omega_forcing;
  global omega_forcing1;
  global omega_forcing2;
  global N_1;
  global N_3;
  global r;
  global n_1;
  global zeta;
  x1 = (-3:0.0001:3);
  N_1 = 4;
  N_3 = 0;
  r = 0;
  zeta = 0.1;
  n_1 = 10;
  Y_U1_lin = N_1*(1-r)/2*x1.^2;
  tau_values = [0 150];
  tauf = 100;
  P_ave_lin = zeros(3,1);
  % case 1 linear
  omega_forcing = 20*2*pi;
  [T1_lin,Y1_lin] = ode45(@nonlin_corr_Case1,tau_values,initial_condition);
  Y1_length = length(Y1_lin);
  total_E1_lin = mean(Y1_lin(Y1_length*0.75:Y1_length,4));
  P_ave_lin(1) = total_E1_lin/tau_values(2);
  % case 2 linear
  omega_forcing1 = 25*2*pi;
  omega_forcing2 = 45*2*pi;
  [tv2_lin,yv2_lin] = ode45(@nonlin_corr_Case2,tau_values,initial_condition);
  yv2_length = length(yv2_lin);
  total_E2_lin = mean(yv2_lin(yv2_length*0.75:yv2_length,4));
  P_ave_lin(2) = total_E2_lin/tau_values(2);
  % case 3 linear
  omega_forcing = 2*pi*randi(100,n_1,1);
  [tv3_lin,yv3_lin] = ode45(@nonlin_corr_Case3,tau_values,initial_condition);
```

```
yv3lin_length = length(yv3_lin);
total_E3_lin = mean(yv3_lin(yv3lin_length*0.75:yv3lin_length,4));
P_ave_lin(3) = total_E3_lin/tau_values(2);

Functions:   function dgamma = nonlin_corr_Case1(tau,gamma)
    global zeta;
    global omega_forcing;
    global N_1;
    global N_3;
    global r;
    dgamma = zeros(4,1);
    dgamma(1) = 8*omega_forcing*sin(omega_forcing*tau);
    dgamma(2) = gamma(3);
    dgamma(3) = -2*zeta*gamma(3) - N_1*(1-r)*gamma(2) - N_3*gamma(2).^3 +
    gamma(1);
    dgamma(4) = zeta*gamma(3).*gamma(3);
  end
  function dgamma = nonlin_corr_Case2(tau,gamma)
    global zeta;
    global omega_forcing1;
    global omega_forcing2;
    global N_1;
    global N_3;
    global r;
    dgamma = zeros(4,1);
    dgamma(1) = 8*omega_forcing1*cos(omega_forcing1*tau) +
      8*omega_forcing2*cos(omega_forcing2*tau);
    dgamma(2) = gamma(3);
    dgamma(3) = -2*zeta*gamma(3)-N_1*(1-r)*gamma(2)-N_3*gamma(2).^3 + gamma(1);
    dgamma(4) = zeta*gamma(3).*gamma(3);
  end
  function dgamma = nonlin_corr_Case3(tau,gamma)
    global zeta;
    global N_1;
    global N_3;
    global omega_forcing;
    global r;
    global n_1;
    dgamma = zeros(4,1);
    dgamma(1) = 0;
    for i = 1:n_1 dgamma(1) = dgamma(1) +
8*omega_forcing(i)*cos(omega_forcing(i)*tau);
    end
    dgamma(2) = gamma(3);
    dgamma(3) = -2*zeta*gamma(3)-N_1*(1-r)*gamma(2)-N_3*gamma(2).^3 - gamma(1);
```

```
  dgamma(4) = zeta*gamma(3).*gamma(3);
end
```

## References


[1] RL Harne and KW Wang. A review of the recent research on vibration energy harvesting via bistable systems. *Smart materials and structures*, 22(2):023001, 2013.

[2] Mohammed F Daqaq, Ravindra Masana, Alper Erturk, and D Dane Quinn. On the role of nonlinearities in vibratory energy harvesting: A critical review and discussion. *Applied Mechanics Reviews*, 66(4):040801, 2014.

[3] S P Beeby, M J Tudor, and NM White. Energy harvesting vibration sources for microsystems applications. *Measurement science and technology*, 17(12):R175, 2006.

[4] Dibin Zhu, Michael J Tudor, and Stephen P Beeby. Strategies for increasing the operating frequency range of vibration energy harvesters: a review. *Measurement Science and Technology*, 21(2):022001, 2010.

[5] F Cottone, H Vocca, and L Gammaitoni. Nonlinear energy harvesting. *Physical Review Letters*, 102(8):080601, 2009.

[6] Samuel C Stanton, Clark C McGehee, and Brian P Mann. Nonlinear dynamics for broadband energy harvesting: Investigation of a bistable piezoelectric inertial generator. *Physica D: Nonlinear Phenomena*, 239(10):640–653, 2010.

[7] D Dane Quinn, Lawrence A Bergman, Alexander F Vakakis, and Angela L Triplett. Comparing linear and essentially nonlinear vibration-based energy harvesting. *Journal of vibration and acoustics*, 133(1):011001, 2011.

[8] A Erturk and DJ Inman. Broadband piezoelectric power generation on high-energy orbits of the bistable duffing oscillator with electromechanical coupling. *Journal of Sound and Vibration*, 330(10):2339–2353, 2011.

[9] Seok-Min Jung and Kwang-Seok Yun. Energy-harvesting device with mechanical frequency-up conversion mechanism for increased power efficiency and wideband operation. *Applied Physics Letters*, 96(11):111906, 2010.

[10] JT Scruggs. An optimal stochastic control theory for distributed energy harvesting networks. *Journal of Sound and Vibration*, 320(4):707–725, 2009.

[11] Shad Roundy and Yang Zhang. Toward self-tuning adaptive vibration-based microgenerators. In *Smart Materials, Nano-, and Micro-Smart Systems*, pages 373–384. International Society for Optics and Photonics, 2005.

[12] Shad Roundy, Eli S Leland, Jessy Baker, Eric Carleton, Elizabeth Reilly, Elaine Lai, Brian Otis, Jan M Rabaey, Paul K Wright, and V Sundararajan. Improving power output for vibration-based energy scavengers. *Pervasive Computing, IEEE*, 4(1):28–36, 2005.

[13] Marco Ferrari, Vittorio Ferrari, Michele Guizzetti, Daniele Marioli, and Andrea Taroni. Piezoelectric multifrequency energy converter for power harvesting in autonomous microsystems. *Sensors and Actuators A: Physical*, 142(1):329–335, 2008.

[14] Haluk Kulah and Khalil Najafi. Energy scavenging from low-frequency vibrations by using frequency up-conversion for wireless sensor applications. *Sensors Journal, IEEE*, 8(3):261–268, 2008.

[15] BP Mann and ND Sims. Energy harvesting from the nonlinear oscillations of magnetic levitation. *Journal of Sound and Vibration*, 319(1):515–530, 2009.

[16] Lihua Tang, Yaowen Yang, and Chee-Kiong Soh. Improving functionality of vibration energy harvesters using magnets. *Journal of Intelligent Material Systems and Structures*, page 1045389X12443016, 2012.

[17] Roszaidi Ramlan, MJ Brennan, BR Mace, and I Kovacic. Potential benefits of a non-linear stiffness in an energy harvesting device. *Nonlinear Dynamics*, 59(4):545–558, 2010.

[18] AF Arrieta, P Hagedorn, A Erturk, and DJ Inman. A piezoelectric bistable plate for nonlinear broadband energy harvesting. *Applied Physics Letters*, 97(10):104102, 2010.

[19] Sergio P Pellegrini, Nima Tolou, Mark Schenk, and Just L Herder. Bistable vibration energy harvesters: A review. *Journal of Intelligent Material Systems and Structures*, 24(11):1303–1312, 2013.

[20] M Ferrari, V Ferrari, M Guizzetti, B Andò, S Baglio, and C Trigona. Improved energy harvesting from wideband vibrations by nonlinear piezoelectric converters. *Sensors and Actuators A: Physical*, 162(2):425–431, 2010.